energies

MDPI

Article

Structural Design, Analysis, and Testing of a 10 kW Fabric-Covered Wind Turbine Blade

Dong-Kuk Choi, Bong-Do Pyeon, Soo-Yong Lee, Hak-Gu Lee and Jae-Sung Bae *

School of Aerospace and Mechanical Engineering, Korea Aerospace University, 200-1 Hwajeon-dong, Deogyang-gu, Goyang-si, Gyeonggi-do 412-791, Korea; dgchoi@kau.kr (D.-K.C.); pringles_1@nate.com (B.-D.P.); leesy@kau.ac.kr (S.-Y.L.); hakgulee@kau.ac.kr (H.-G.L.)

* Correspondence: jsbae@kau.ac.kr

Received: 5 April 2020; Accepted: 19 June 2020; Published: 24 June 2020

Abstract: Reducing the weight of a wind turbine blade is a major issue. Wind turbines have become larger in size to increase power generating efficiency. The blade has also grown in length to take more wind energy. A fabric-based wind turbine blade, introduced by General Electric Co., reduced the blade weight. In this study, a small fabric-covered blade for a 10 kW wind turbine was developed to verify structural ability. The blade was designed on the cross-section using variational asymptotic beam sectional analysis (VABS), structural analysis was carried out using MSC.Nastran for the design loads. A modal analysis was performed to compare the modal frequency and mode shapes. Static structural testing and modal testing were fulfilled. The analysis results were compared with the testing results. The fabric-covered structure was confirmed to reduce the blade mass with sufficient strength.

Keywords: wind energy; wind turbine; blade; fabric-covered blade; structural testing; VABS

1. Introduction

While wind turbines have increased in length and weight, wind turbine blades have faced challenges such as construction, transportation, and installation [1–5]. General Electric (GE) Co. and the National Renewable Energy Laboratory (NREL) have introduced a fabric-covered wind turbine blade [6] that reduces the weight and manufacturing cost of wind turbine blades. The fabric-covered blade, as shown in Figure 1, is similar to an aircraft wing and its skin is made from fabric materials. The fabric-covered blade is able to reduce weight and achieve modularization [6,7]. GE [8] studied several types of truss structure blades with tensioned fabric skin. Their blade structure did not save weight because the added mass required modifications to maintain the buckling margins. Bae et al. [9,10] studied the 5 MW fabric-covered blade to verify whether the structure could be adapted to a large wind turbine blade. They predicted a reduction in blade weight of over 30%, although their research was preliminary. Choi et al. [11] designed and analyzed a fabric-covered wind turbine blade structure. The authors performed static structural analysis and buckling analysis, and they proposed a spar structure for a fabric-covered blade. They concluded that the fabric-covered blade structure would reduce blade weight by up to 36%. However, previous authors have only carried out numerical analyses. An experimental study of fabric-covered blades is therefore needed to confirm that the structural ability would be dissimilar to typical wind turbine blades.

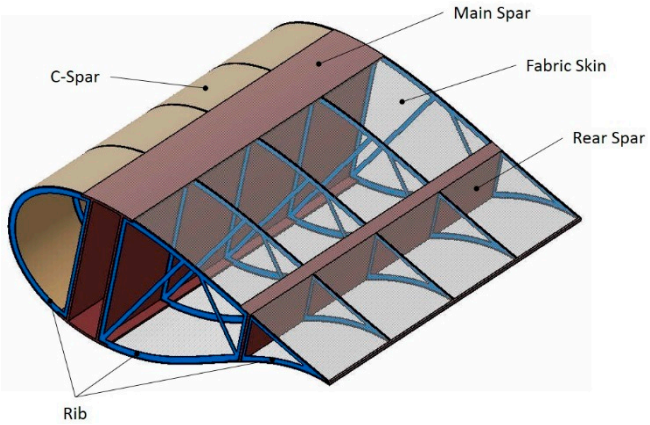

Figure 1. The concept of a fabric-covered wind turbine (WT) blade.

Wind turbine blades should be structurally tested for new development. Fagan et al. [12] designed and tested a specific 15 kW turbine blade. The blade design was based on the non-dominated sorting genetic algorithm and the numerical model was built using Abaqus. A whiffle tree test rig was used in the structural testing of the blade. The difference between the predicted and measured results were 13% in mass and 18% in deflection. Yang et al. [13] carried out an actual collapse testing under flapwise loading for a large-scale composite wind turbine blade with a 40 m length. The flapwise load was obtained by applying shear force at four locations. The test results showed that the final failure occurred at 160% of the extreme design load. Kong et al. [14] investigated the structural design and testing for a 750 kW wind turbine blade. The test load was applied at three positions. The analysis results showed a 3% difference compared with the testing results. Paquette et al. [15] tested three types of 9 m carbon fiber composite wind turbine blades where the blades were loaded with a three-point whiffle-tree arrangement. The three types of blades were compared with each other. Many researchers have studied structural testing and numerical analysis, but their research has been limited to typical wind turbine blades [12–18], thus the structural testing of fabric-covered blades is urgently needed.

This study investigated the structural design and testing of a fabric-covered wind turbine blade to confirm that the structure could reduce the blade mass while retaining sufficient strength. A small 10 kW wind turbine blade was selected because such a blade can be built and tested in a university laboratory. Structural behavior and normal mode were analyzed using variational asymptotic beam sectional analysis (VABS) and MSC.Nastran. Static and normal mode testing were performed. Finally, the analysis results were compared with the testing results.

2. Structural Design

2.1. Blade Shape

The blade's aerodynamic shape was designed by the Korea Institute of Energy Research [19] as shown in Figure 2. The blade's overall length was 3.55 m, the maximum chord length was 0.35 m, root diameter was 0.2 m, and the maximum twist angle was 20 degrees.

Figure 2. The aerodynamic shape of the blade.

Figure 3 presents the structurally designed blade. The blade had a 0.35 m length root, a 2.91 m main structure, and a 0.29 m length tip. The root was a composite shell structure similar to a typical wind turbine blade. The main structure was composed of a C-spar, main spar, rear spar, ribs, root

shell, and root mount. The spar design is explained in Section 2.3. The rib structure and the blade structure analysis model are described in Section 2.4. Figure 4 shows the finally designed and fabricated fabric-covered blade in this paper. The blade weight was 7.80 kg without the skin and tip. Table 1 is a list of the components' mass.

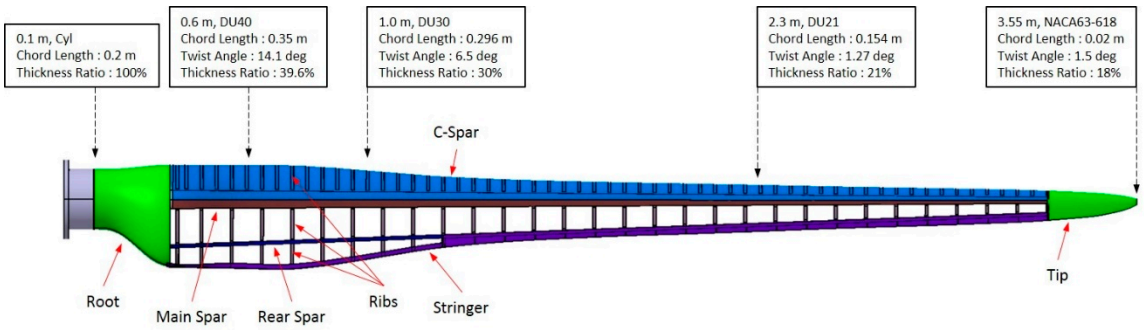

Figure 3. The fabric-covered blade structure.

(**a**) (**b**)

Figure 4. The fabricated fabric-covered blade: (**a**) without skin and (**b**) with skin.

Table 1. The components' mass of the fabric-covered blade.

Component	C-Spar	Main Spar	Rear Spar	Ribs	Root	Stringer	Adhesive (Estimated)	Total
Mass (kg)	0.34	2.21	0.20	0.53	4.08	0.06	0.38	7.80

2.2. Design Load Case

The blade load cases were selected from the International Electrotechnical Commission (IEC) 61400-1 Ed.3 Design Load Cases (DLC) [20]. The simulated wind conditions and details are listed in Table 2. The blade loads were calculated using FAST code [21]. The V_{hub} of DLC 1.1, 1.3, and 1.5 ranged from 4 m/s to 25 m/s at 2 m/s interval. The rated wind speed V_r was 9.5 m/s. Dash-lines in Figure 5 are the simulated results, and solid-lines with circles are the maximum and minimum values of all calculated cases. The partial safety factors were applied at 1.35 for simulated loads and 1.1 for materials. Figure 6 shows the design loads applied for the safety factors. The present study did not deal with unsteady loadings by atmospheric turbulence, wake turbulence, etc. The information about the unsteady loading can be referred to in works by Churchfield et al. [22] and Nandi et al. [23].

Table 2. Design load cases.

Design Situation	DLC	Wind Condition
Power production	1.1	NTM $V_{in} < V_{hub} < V_{out}$
	1.3	ETM $V_{in} < V_{hub} < V_{out}$
	1.4	ECD $V_{hub} = V_r \pm 2$ m/s
	1.5	EWS $V_{in} < V_{hub} < V_{out}$
Normal shut down	4.2	EOG $V_{hub} = V_r \pm 2$ m/s and V_{out}
Emergency shut down	5.1	NTM $V_{hub} = V_r \pm 2$ m/s and V_{out}
Parked	6.1	EWM 50-year recurrence period

NTM: Normal Turbulence Model; ETM: Extreme Turbulence Model; EC: Extreme Coherent gust with Direction change; EOG: Extreme Operating Gust; EWM: Extreme Wind speed Model; V_{in}: cut-in wind speed; V_{out}: cut-out wind speed; V_r: rated wind speed; V_{hub}: wind speed at hub height.

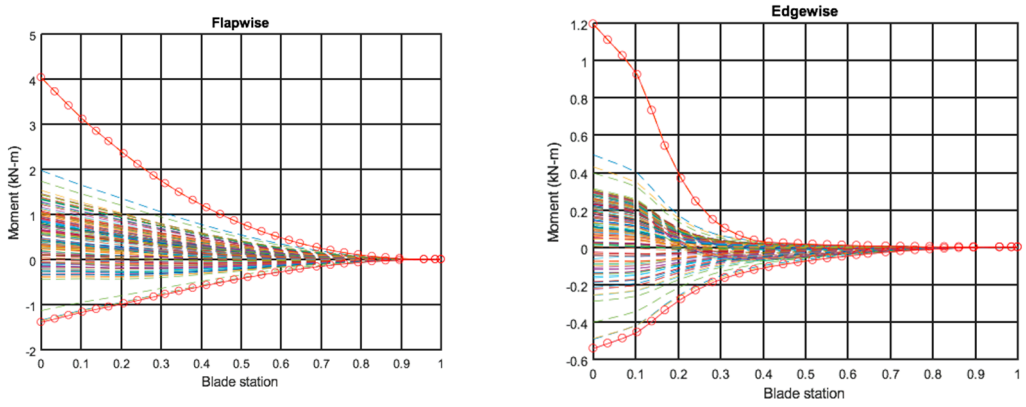

(**a**) (**b**)

Figure 5. The simulated loads: (**a**) flapwise direction and (**b**) edgewise direction.

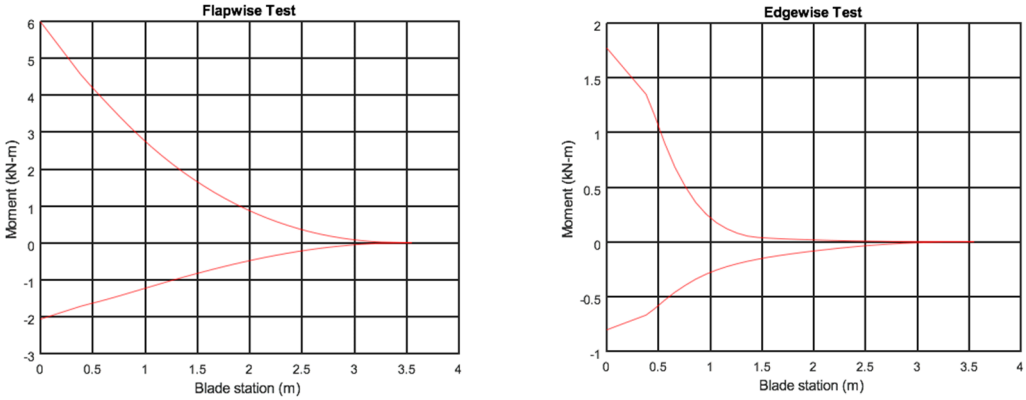

(**a**) (**b**)

Figure 6. The design loads: (**a**) flapwise direction and (**b**) edgewise direction.

2.3. 2D Cross-Sectional Design of the Spar

The blade spar was designed by applying a cross-sectional analysis method. The cross-sectional properties and stress analysis were calculated using VABS [24], and pre/post-process were performed by applying in-house MATLAB-based codes. The applied carbon composite materials were LCU250NS

and CF3327, which are products of Hankuk Carbon Co. The basic physical property tests were performed to obtain the carbon composite materials characteristics, as shown in Table 3.

Table 3. Properties of the carbon composite materials.

	LCU250NS	CF3327
E_1 (GPa)	118.0	54.90
E_2 (GPa)	8.3	57.95
G_{12} (GPa)	3.85	3.30
ν_{12} (-)	0.33	0.065
X_T (MPa)	2005	566.8
Y_T (MPa)	39	579.4
X_C (MPa)	978	414.4
Y_C (MPa)	162	410.8
Shear Strength (MPa)	85	99.1

The designed spar was composed with a C-spar, main spar and rear spar. The main spar caps that experience flapwise bending moments have the stacking sequence $[(0)_2/\pm45/(0)_5/\pm45/(0)_6]$ from root to 2.535 m and $[0/0/\pm45/0/0]_s$ from 2.535 m to 3.26 m, as shown in Figure 7. The main spar web that sustains shear loads has the stacking sequence $[0/0/\pm45/0]_s$. The C-spar that also sustains shear loads during torsion has the stacking sequence [±45]. The rear spar that mainly experiences edgewise bending moment has the stacking sequence [0/±45/0].

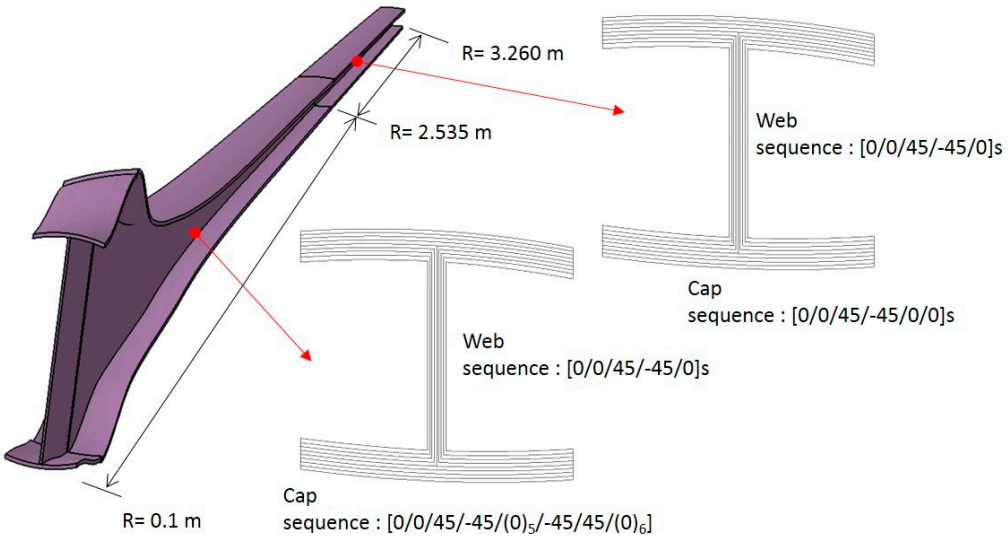

Figure 7. Main spar cross-section and stacking sequence.

Figure 8 shows the cross-sectional analysis results applied to Tsai–Wu failure criteria under design loads. The maximum failure index was 0.52 between the main spar cap and the web at the R = 1.59 m location. The results show that the blade structure is safe under the design loads.

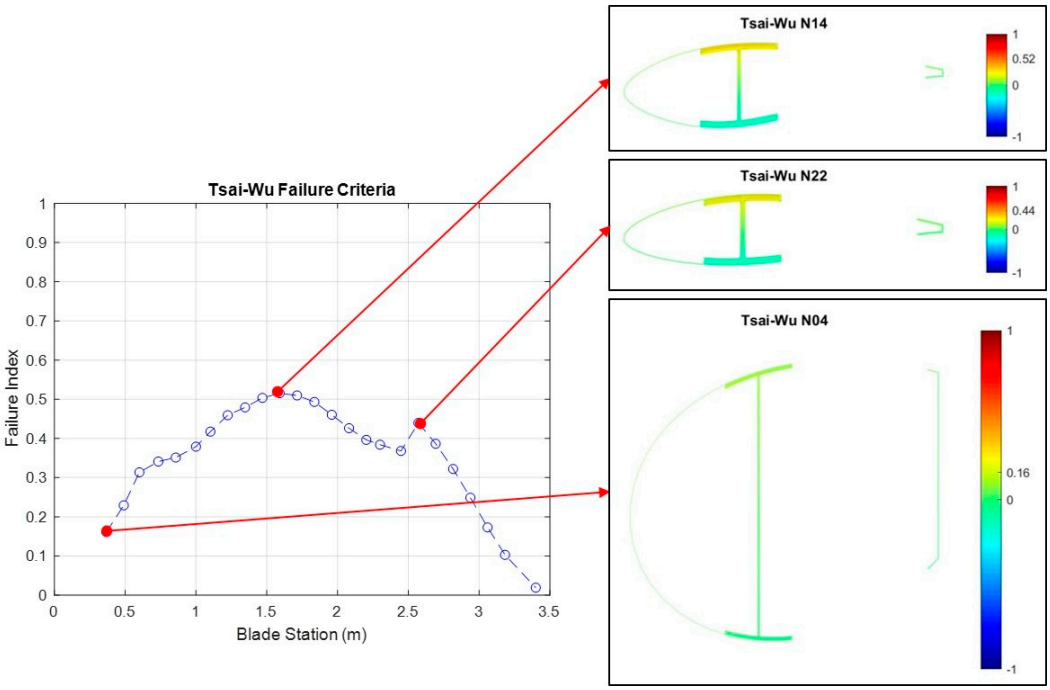

Figure 8. The maximum failure indexes of the cross-sections along the blade span.

2.4. 3D Finite Element Model of the Blade

The 3D finite element (FE) model was built from the results of the 2D cross-sectional design. The spars were joined to each other by ribs. The leading edge ribs that exist in between the C-spar and main spar retain the aerodynamic shape of the blade along with C-spar. The middle ribs connect the main spar and rear spar. The trailing edge ribs are placed on the trailing edge of the blade and forms the rear end shape with a thin composite skin. The middle and trailing edge ribs have a distance of 100 mm from each other. The leading edge ribs have a space of 50 mm, because it is necessary to keep the shape of the blade leading edge for aerodynamic characteristics. The ribs have a stacking sequence of [0/±45/0] and the applied material was CF3327. The ribs have an L-shape flange to increase stiffness. Some ribs that have sufficient airfoil thickness take a truss structure in order to reduce the mass. Figure 9 shows a rib applied to a truss structure. The fabric skin was not included in this model because the skin did not sustain the loads and it only maintains the aerodynamic shape.

Figure 9. The truss ribs.

Finally, the 3D blade FE analysis model is shown in Figure 10. The FE analysis model had 33,345 CQUAD4 elements. The design loads were applied to each rib position, for a total of 30 points. The root material was applied to the aluminum alloy 6061-T6 (MAT1, PSHELL), and the rest were applied to

carbon composite materials (MAT8, PCOMP). The static analyses were performed with the maximum and minimum loads.

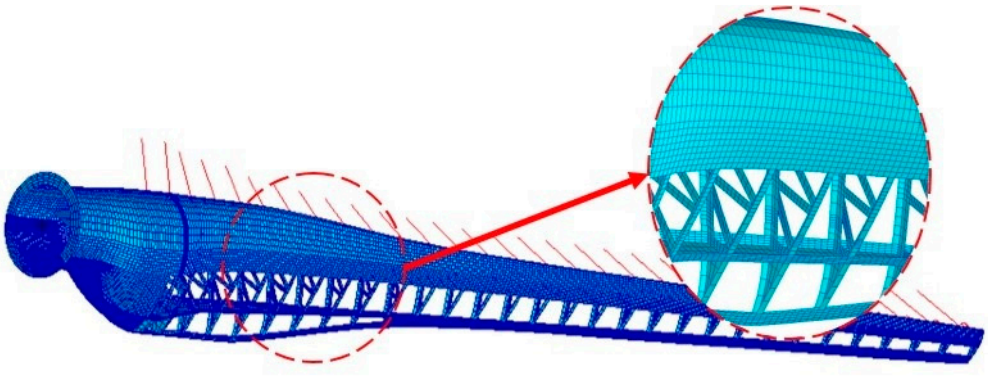

Figure 10. The 3D blade finite element model.

Figure 11 shows the blade displacement and Tsai–Wu failure indexes under the maximum load cases. The blade displacements were flapwise 182 mm and edgewise −12.6 mm under the maximum design load. The maximum failure index was 0.48 at blade location R = 0.610 m. Therefore, the designed blade structure has sufficient strength.

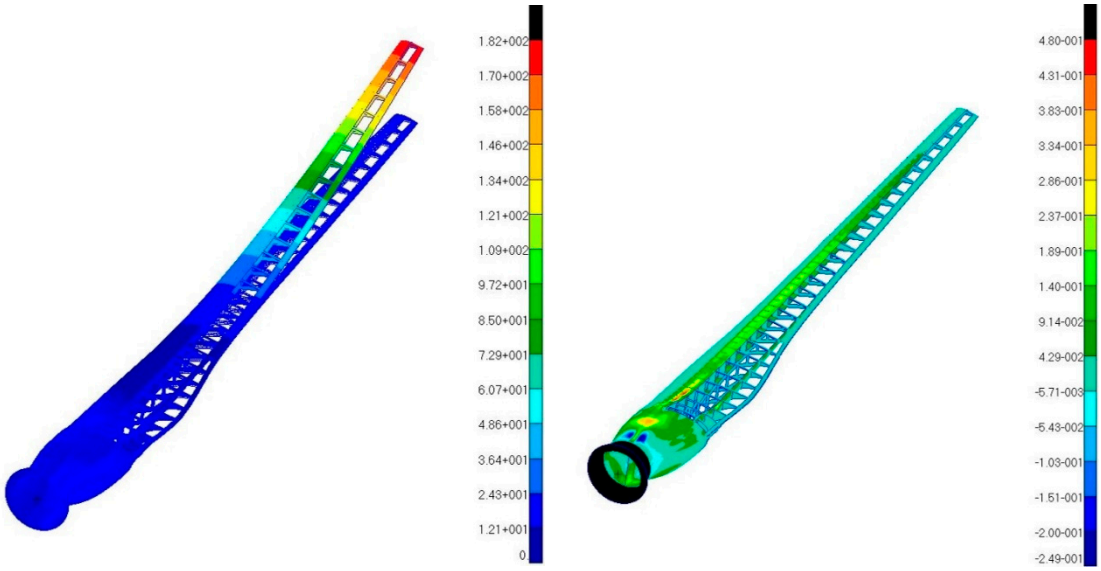

(**a**) (**b**)

Figure 11. The structural analysis results of the 3D blade model: (**a**) deflection and (**b**) Tsai–Wu failure criteria indexes.

3. Modal Test

3.1. Test Apparatus

The modal test apparatus was composed of uniaxial acceleration sensors, an impact hammer, and a DAQ system. Table 4 shows the equipment list for the modal test. The uniaxial acceleration sensors convert the acceleration with flapwise and edgewise direction to an electric signal. The impact hammer applies an excitation to the blade. The DAQ system measures the acceleration data while the blade is vibrating.

Table 4. The equipment list for modal testing.

Equipment	Specification
Acceleration sensor	Uniaxial type
Impact hammer	B&K 8206
DAQ system	dSPACE 1103

3.2. Test Setup and Procedure

The modal testing was set to the free–free condition. The uniaxial acceleration sensors were attached to the blade with spacing of 500 mm, as shown in Figure 12. Each of the six acceleration sensors (a total of 12 sensors) were used to determine the flapwise and edgewise frequency and mode shapes. The excitation point was located at 1400 mm from the root. The DAQ system measures the acceleration sensor data with a sampling rate of 2000 sample/s. The time based acquired data were transformed to the frequency domain by Fast Fourier Transform (FFT).

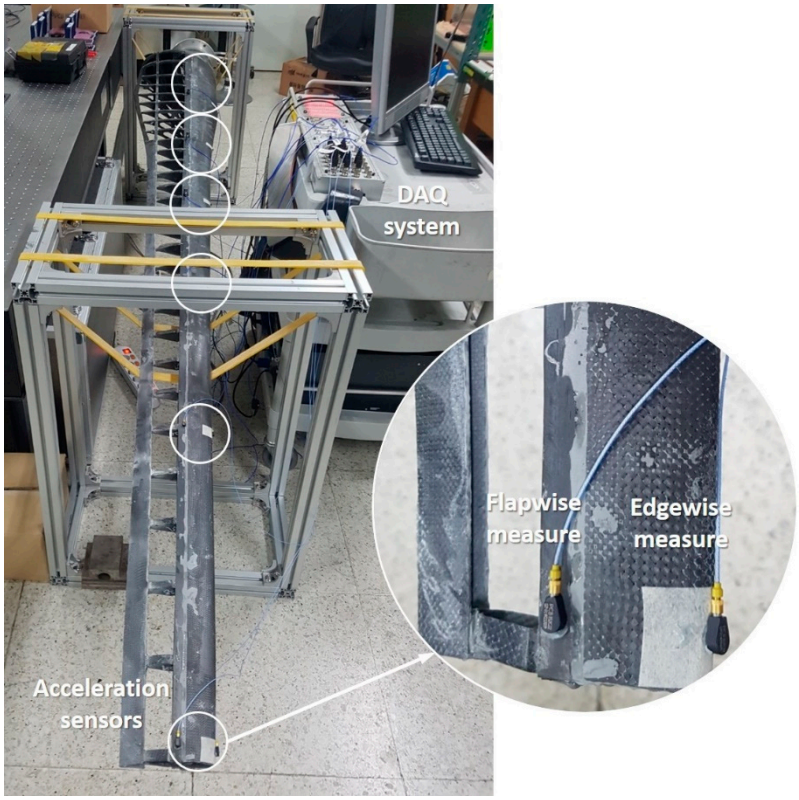

Figure 12. The modal test setup.

4. Structural Test

4.1. Test Apparatus

The test apparatus was mainly composed of a test stand, hydraulic actuator, loadcell, wire displacement sensors, DAQ system, and control equipment, as shown in Figure 13. Table 5 shows the equipment list for the structural testing. The hydraulic actuator makes a load. A wire and pulley deliver the load to the blade from the hydraulic actuator. The loadcell is located on the cylinder of hydraulic actuator. The wire displacement sensors are placed above the blade and linked to the loading fixture. The DAQ system measures the loads and displacements during structural testing. The control equipment manages the hydraulic system in the test steps.

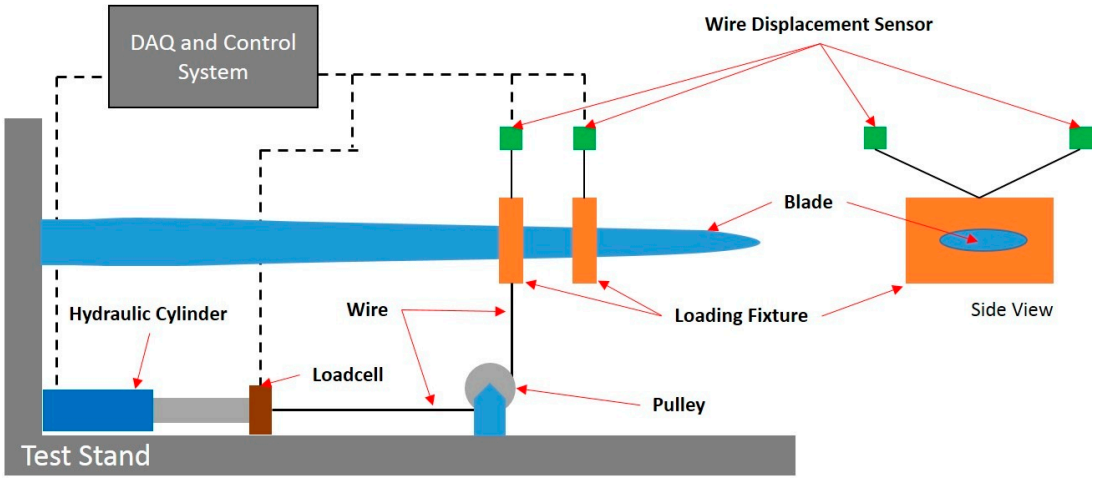

Figure 13. The static structural testing equipment configuration.

Table 5. The equipment list for the static structural testing.

Equipment	Specification
Test stand	-
Loadcell	DACELL 1 ton
Wire displacement sensor	1.2 m range
Winch system	Hydraulic cylinder
Loading fixture	-
DAQ system	NI PCI-6014

4.2. Test Load Case

The structural static tests were carried out at the maximum and minimum loads in the flapwise and edgewise directions. The dotted lines in Figure 14 are the maximum and minimum design loads, and the solid lines are test loads. Each testing direction, except the flapwise minimum load case, was divided by two cases to match with the bending moment level of design loads because the load was applied to one location on the blade. The flapwise minimum load could be set as one test case. Figure 15 shows the test loads at the loading position. There was a total of seven testing cases, as listed in Table 6.

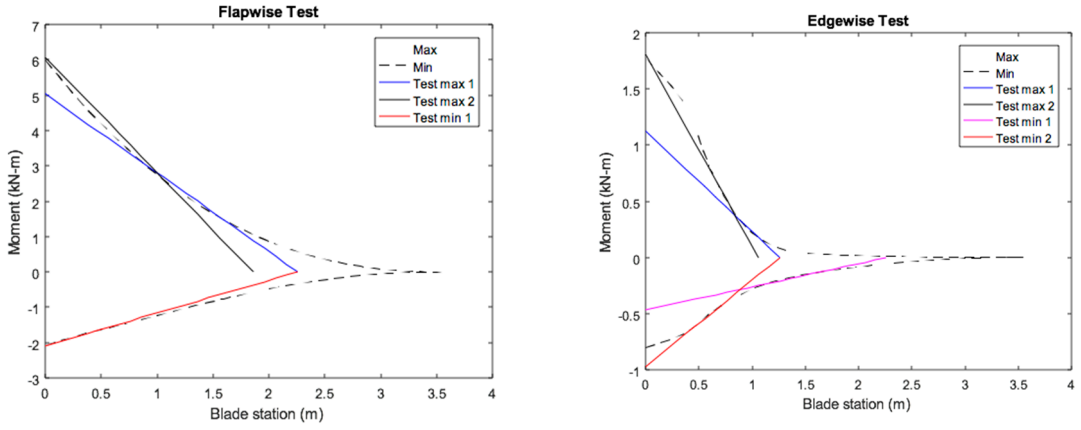

(**a**) (**b**)

Figure 14. The test loads: (**a**) flapwise direction and (**b**) edgewise direction.

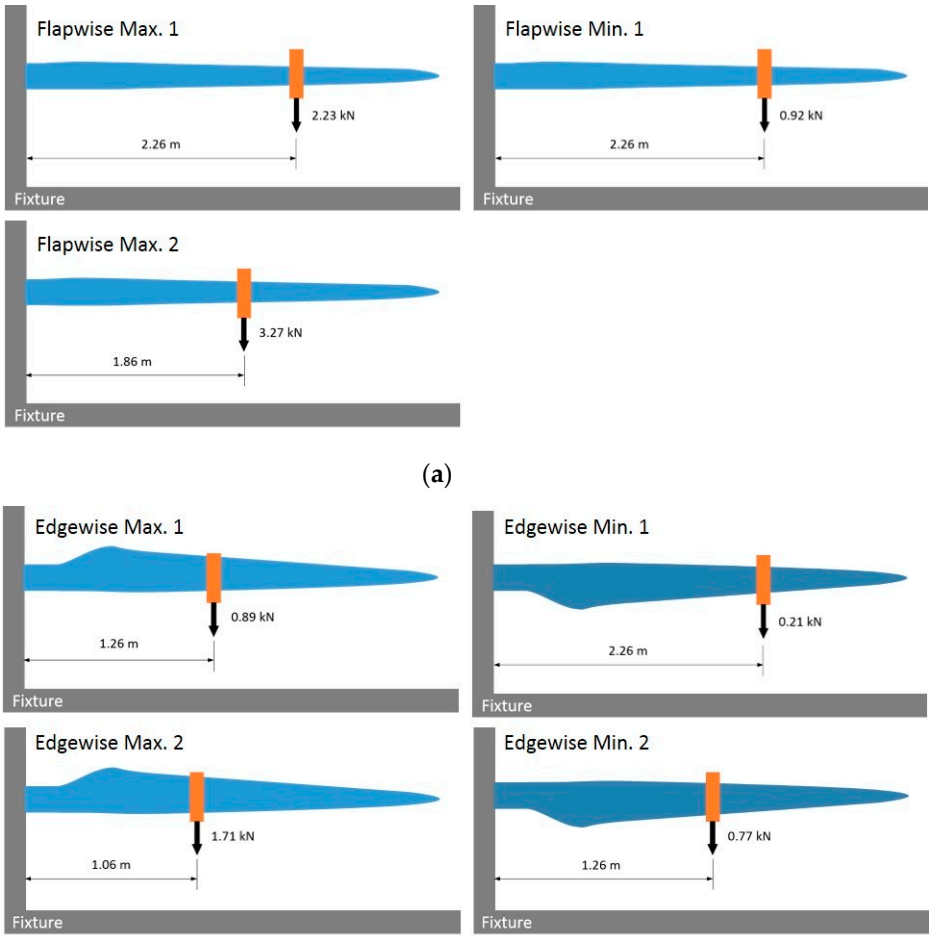

Figure 15. The test cases with testing loads at loading position: (**a**) flapwise direction and (**b**) edgewise direction.

Table 6. The test cases.

Case	Quantity Description
Case 1	Flapwise maximum load 1 (loading 2.23 kN at 2.26 m)
Case 2	Flapwise maximum load 2 (loading 3.27 kN at 1.86 m)
Case 3	Flapwise minimum load (loading 0.92 kN at 2.26 m)
Case 4	Edgewise maximum load 1 (loading 0.89 kN at 1.26 m)
Case 5	Edgewise maximum load 2 (loading 1.71 kN at 1.06 m)
Case 6	Edgewise minimum load 1 (loading 0.21 kN at 2.26 m)
Case 7	Edgewise minimum load 2 (loading 0.77 kN at 1.26 m)

4.3. Test Setup and Procedure

The global coordinate system was defined and used for the blade static test. It was fixed on the test stand. The origin of the global coordinate system was located at the center of the blade root. The *x*-axis is defined as the global horizontal line and directed to the right side when seeing the blade tip to root. The *y*-axis is defined as the global vertical line to the ground and is directed upside. The *z*-axis is defined as the line from the root to tip. The blade coordinate system is defined at the center of the

blade root. The *y*-axis is defined as the line that is parallel with the chord line at the zero-twist blade station, and is directed to the trailing edge of the blade. The *z*-axis is defined as the line from the root to tip along the pitch axis of the blade. The *x*-axis is determined by the right hand rule. The global coordinate system and the blade coordinate system are shown in Figure 16.

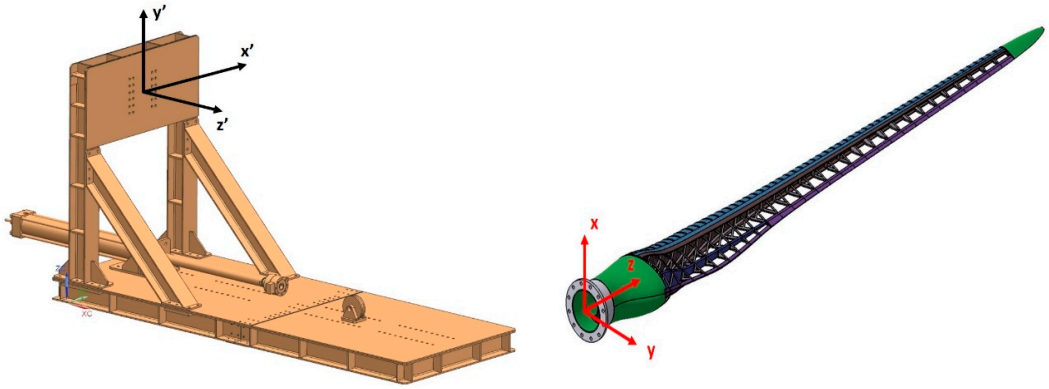

(**a**) (**b**)

Figure 16. The coordinate system: (**a**) the global coordinate system and (**b**) the blade coordinate system.

When mounting the test blade on the test stand, the blade coordinate system was matched with the global coordinate system for the maximum edgewise test. For the maximum flapwise, minimum edgewise, and minimum flapwise test, the blade was rotated each −90°, 180°, and 90°. The structural testing was set up for the test equipment and the blade, as shown in Figure 17.

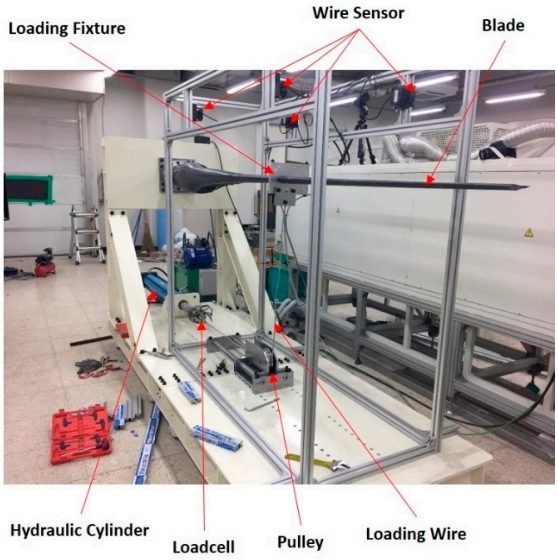

Figure 17. The test setup.

The structural test procedure had 12 steps. The load was applied in a total of five steps. The following is the test process.

1. Fixing the blade to the test stand.
2. Mounting the loading fixture at the location.
3. Performing the zero setting of the loadcell before connecting to the loading fixture.
4. Connecting the winch wire with the loading fixture and loadcell.
5. Increasing the load up to the 40%, 60%, 80%, 90%, and 100% level of the test load, and then maintaining the load for 15 s at each load level.

5. Result of Analysis and Testing

5.1. Modal Analysis and Testing

The modal analysis and testing were performed for the free–free condition. The uniaxial acceleration sensors measured flapwise and edgewise acceleration with each of the six sensors, for a total of 12 sensors. The impact hammer applied excitation to the blade. Figure 18a,b shows the sensor data during the modal test. The frequency response results are represented in Figure 18c,d. The first mode was the flapwise first bending mode with 30.52 Hz frequency, as shown in Figure 19a. The second and third mode were edgewise first and second bending mode with 39.31 Hz and 80.57 Hz frequencies, respectively, as shown in Figure 19b,c. The fourth mode was the flapwise second bending mode with the 91.31 Hz frequency, as shown in Figure 19d. The tested and simulated modal frequencies are listed in Table 7. The difference between the experimental results and analysis results was within 7.37%. Therefore, it can be said that the numerical model has the equivalent structural characteristics to the fabricated blade.

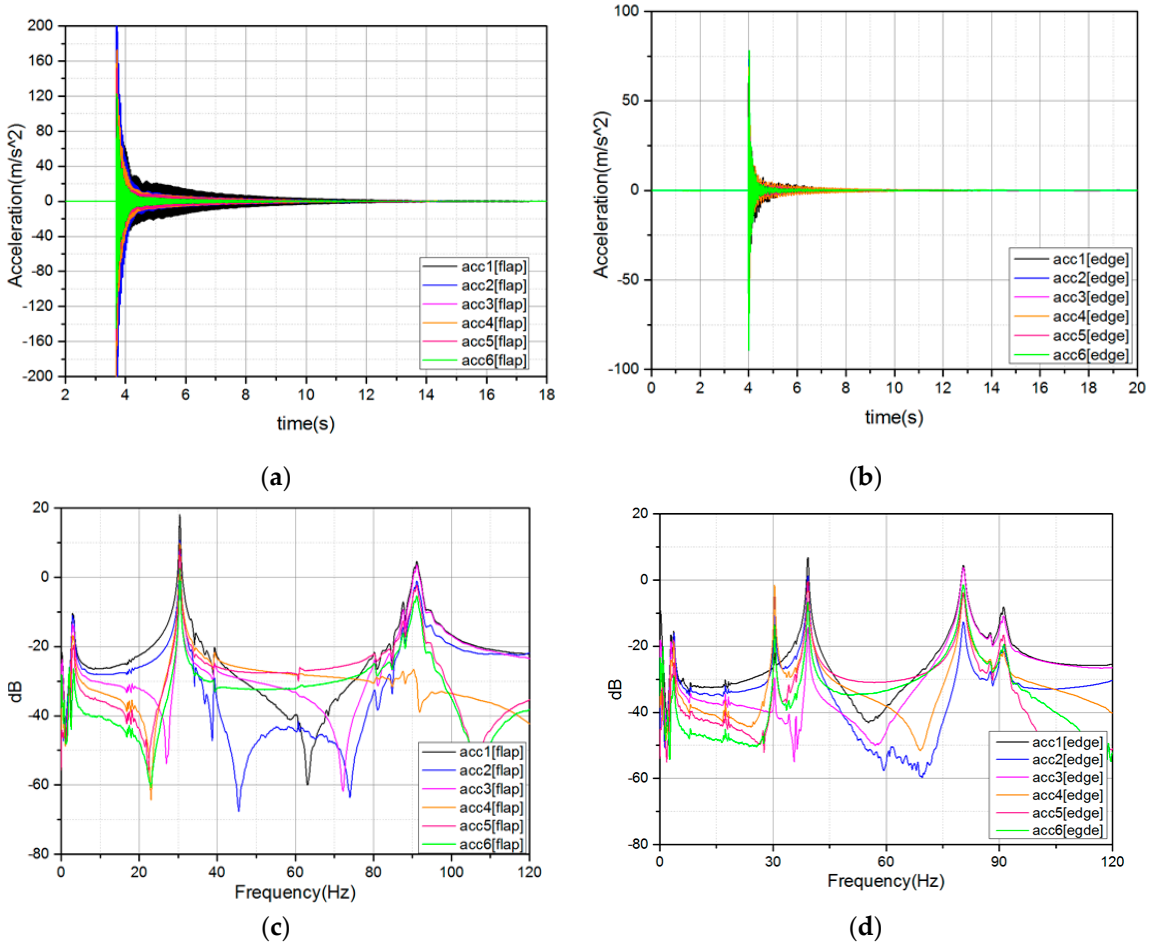

Figure 18. Modal testing results: (**a**) time signal(flapwise), (**b**) time signal(edgewise), (**c**) frequency response(flapwise), and (**d**) frequency response(edgewise).

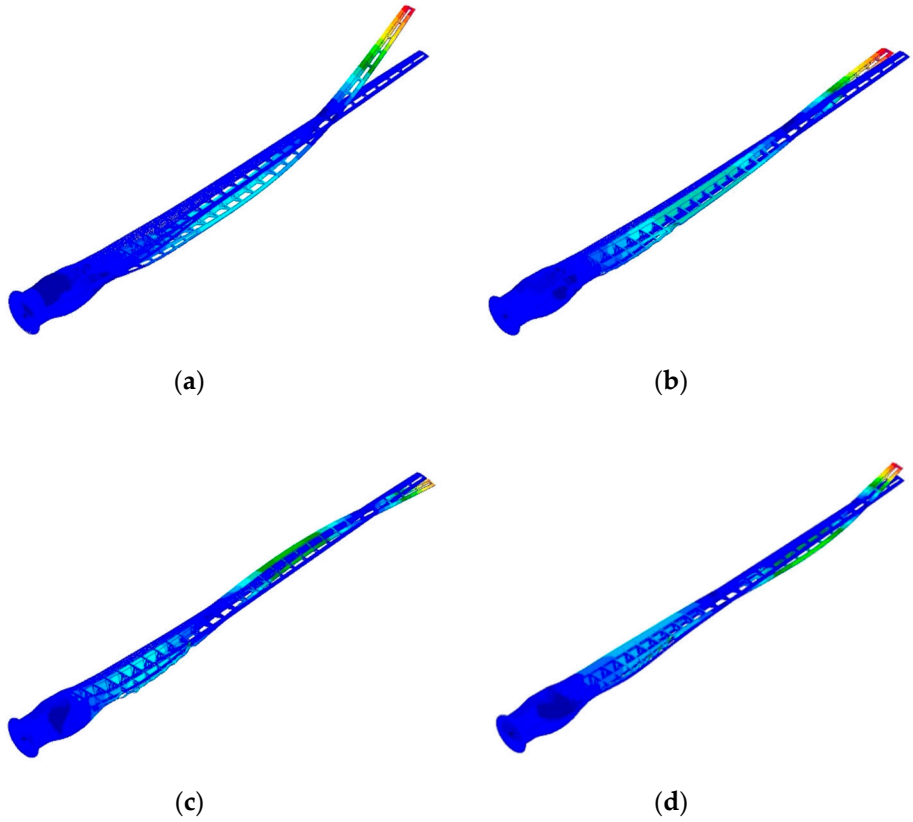

Figure 19. The mode shapes: (**a**) first mode, (**b**) second mode, (**c**) third mode, and (**d**) fourth mode.

Table 7. The experimental and numerical modal frequencies.

Mode	Experiment (Hz)	Numerical (Hz)	Error (%)	Mode Shape
1	30.52	32.77	7.37	first flapwise bending
2	39.31	39.90	1.50	first edgewise bending
3	80.57	83.10	3.14	first edgewise bending
4	91.31	94.73	3.75	second flapwise bending

5.2. Structural Analysis and Testing

Figure 20 shows the structural testing and analysis results. The flapwise test results showed linear behavior, because the flapwise load was mainly sustained on the main spar, which had a thick laminate, as shown in Figure 20a–c. The flapwise analysis cases were within an 8.0% error compared with the flapwise test cases.

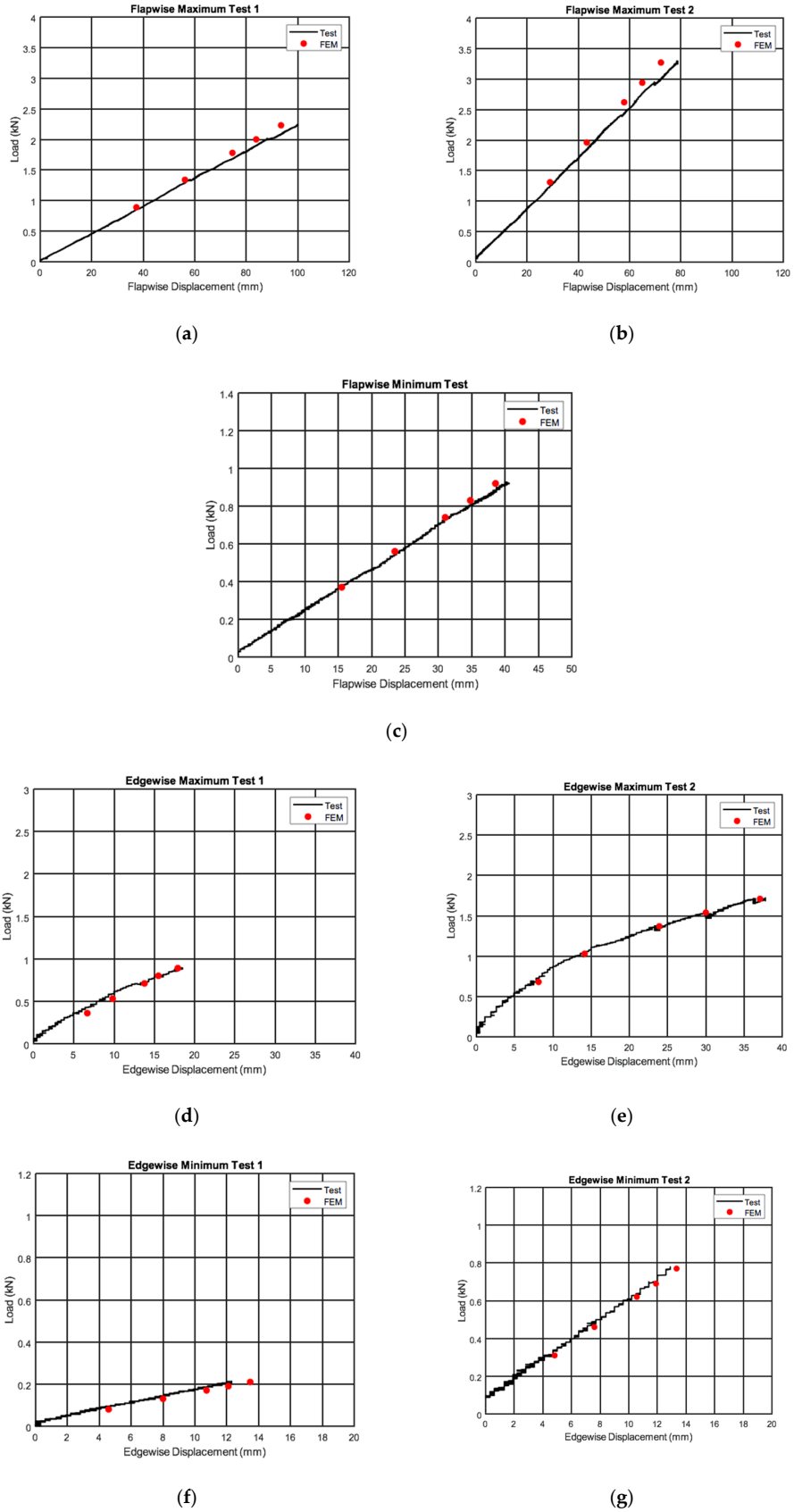

Figure 20. The structural testing and analysis results: (**a**) case 1, (**b**) case 2, (**c**) case 3, (**d**) case 4, (**e**) case 5, (**f**) case 6, and (**g**) case 7.

The edgewise test results showed linear and nonlinear behavior as shown in Figure 20d–g. The results of test cases 4, 6, and 7 had linear load-displacement curve, which were applied to smaller loads than that in test case 5. In test case 5, some of the ribs connected to the main spar and the rear spar sustained bending forces, as shown in Figure 21. Figure 22a shows a load-displacement curve for a rib bending test result. The curve had an initial linear region and final nonlinear region. The rib linear bending analysis result is shown in Figure 22b. The rib displacement was 6.8 mm on the load 60 N. The linear analysis result was well matched with the linear region of the rib test result. Therefore, nonlinearity of the rib must be considered in edgewise load conditions. The rib was analyzed for the nonlinear model or reduced stiffness for applied loads. In this study, some rib flanges were modeled to the membrane element because the rib experiencing buckling did not sustain compressive force by bending. The modified rib model could be simulated to nonlinearity, as shown in Figure 20e. The analysis error in the edgewise cases was 9.5% compared with the test results.

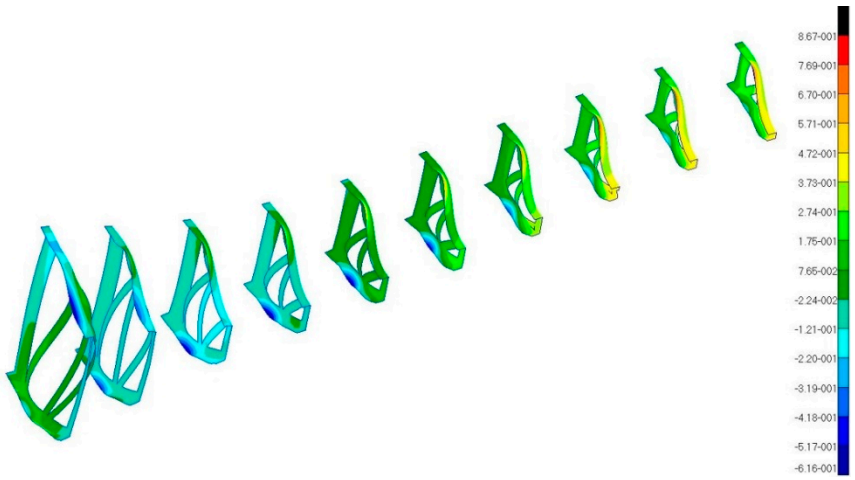

(**a**)

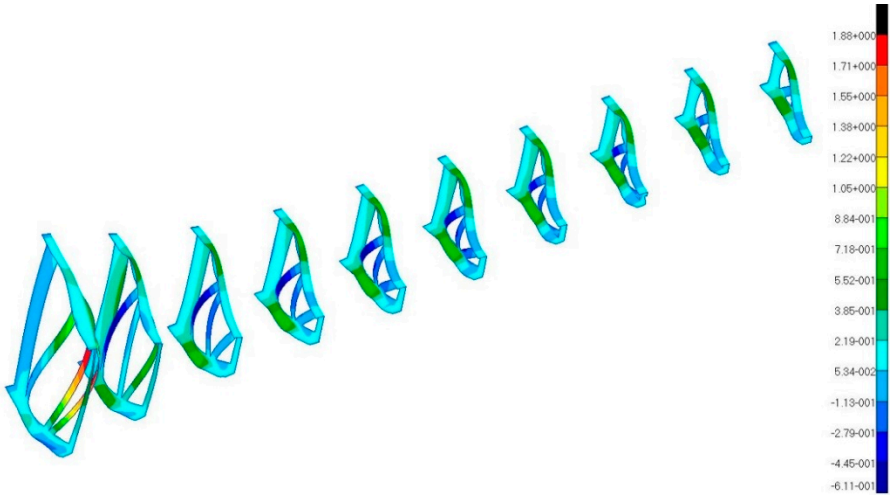

(**b**)

Figure 21. The rib deflection on the edgewise maximum load: (**a**) x-direction fringe and (**b**) z-direction fringe.

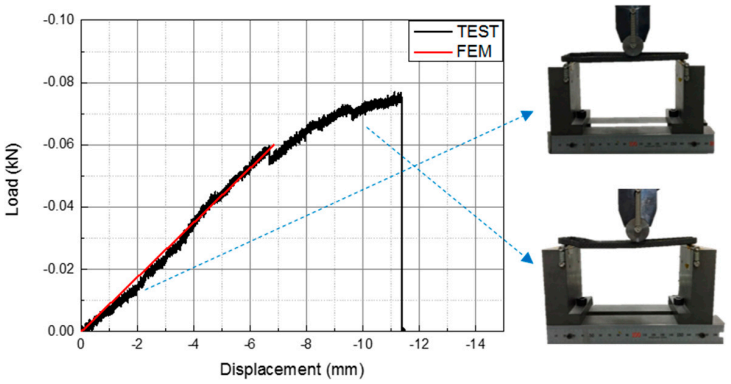

(**a**)

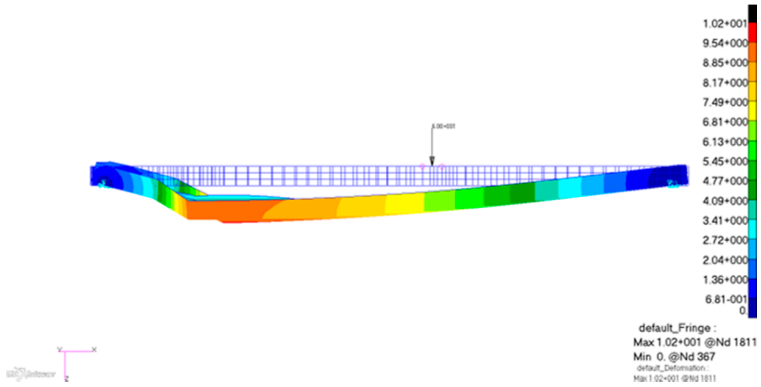

(**b**)

Figure 22. The rib bending test and analysis results: (**a**) testing results and (**b**) numerical results.

To reduce the nonlinearity of the ribs, the thickness has to be increased or the cross-section of the truss member in the rib to become L or C types. However, the increased thickness increases the blade weight, and the modification of the cross-section to L or C type makes the fabrication of the ribs more complex. To avoid these difficult challenges, the nonlinear behavior of ribs due to edgewise loading should be considered when analyzing the fabric-covered blade.

6. Conclusions

A fabric-covered blade was designed for the design load cases (DLC). Structural static and modal testing were carried out, and the testing results were compared with the numerical results. The fabric-covered blade behaved linearly in the flapwise direction. The edgewise behavior was shown nonlinearly, because the ribs sustained bending forces. To consider this phenomenon, nonlinear analysis is needed, or some ribs can be modeled to the membrane elements. The maximum displacement is predicted if all ribs are modeled to the membrane elements. The difference between the testing results and numerical analysis was within 9.45%.

In this study, the fabric-covered blade was confirmed to reduce the structural weight while retaining sufficient strength. Although this work studied a small wind turbine blade, the fabric-frame structure could be applied to a large wind turbine blade.

Author Contributions: Conceptualization, J.-S.B. and D.-K.C.; methodology, D.-K.C. and H.-G.L.; software, D.-K.C. and B.-D.P.; validation, S-.Y.L. and J.-S.B.; formal analysis, D.-K.C.; investigation, D.-K.C.; resources, S.-Y.L. and H.-G.L.; data curation, D.-K.C. and B.-D.P.; writing—original draft preparation, D.-K.C.; writing—review and editing, S.-Y.L., H.-G.L. and J.-S.B.; visualization, J.-S.B.; supervision, S.-Y.L. and J.-S.B.; project administration, J.-S.B.; funding acquisition, J.-S.B. All authors have read and agreed to the published version of the manuscript.

Funding: This research received no external funding.

Acknowledgments: This work was supported by the New & Renewable Energy Core Technology Program of the Korea Institute of Energy Technology Evaluation and Planning (KETEP) granted financial resource from the Ministry of Trade, Industry & Energy, Republic of Korea. (No. 20143030021130).

Conflicts of Interest: The authors declare no conflict of interest.

References

1. McKenna, R.; vd Leye, P.O.; Fichtner, W. Key challenges and prospects for large wind turbines. *Renew. Sustain. Energy Rev.* **2016**, *53*, 1212–1221. [CrossRef]
2. Cotrell, J.; Stehly, T.; Johnson, J.; Roberts, J.O.; Parker, Z.; Scott, G.; Heimiller, D. *Analysis of Transportation and Logistics Challenges Affecting the Deployment of Larger Wind Turbines: Summary of Results*; NREL/TP-5000-61063; National Renewable Energy Laboratory: Golden, CO, USA, 2014.
3. Maples, B.; Saur, G.; Hand, M. *Installation, Operation, and Maintenance Strategies to Reduce the Cost of Offshore Wind Energy*; NREL/TP-5000-57403; National Renewable Energy Laboratory: Golden, CO, USA, 2013.
4. Ren, Z.; Jiang, Z.; Skjetne, R.; Gao, Z. Development and application of a simulator for offshore wind turbine blades installation. *Ocean Eng.* **2018**, *166*, 380–395. [CrossRef]
5. Zhao, Y.; Cheng, Z.; Sandvik, P.C.; Gao, Z.; Moan, T.; van Buren, E. Numerical modeling and analysis of the dynamic motion response of an offshore wind turbine blade during installation by a jack-up crane vessel. *Ocean Eng.* **2018**, *165*, 353–364. [CrossRef]
6. Fang, B.; Olson, S.H.; Lin, W.W.; Krishnamurthy, S.; Haridasu, B.; Kashiram, P.; Daggumati, S.; Subramanian, S.; Finn, S.R.; Kulmi, U.; et al. Wind Turbine Rotor Blade with Fabric Skin and Associated Method for Assembly. U.S. Patent US13/664,603, 31 October 2012.
7. Wetzel, K.K. *Design and Manufacturing of Modular Wind Turbine Blades*; Wetzel Engineering Inc.: Austin, TX, USA, 2015.
8. *ARPA-E Tensioned Fabric Wind Blades*; GE Power and Water: Atlanta, GA, USA, 2014.
9. Bae, J.-S.; Choi, D.-G.; Lee, S.-Y.; Yoo, C.; Kim, D.-J. Preliminary study on a fabric-covered wind turbine blade. In Proceedings of the 4th International Conference on Renewable Energy Research and Applications, Palermo, Italy, 22–25 November 2015.
10. Bae, J.-S. Feasibility study on a fabric-covered wind turbine blade. In Proceedings of the World Congress and Exhibition on Wind and Renewable Energy, Berlin, Germany, 28–30 July 2016.
11. Choi, D.-G.; Kwak, C.-H.; Lee, S.-Y.; Bae, J.-S.; Lee, H.-G. Structural design and analyses of a fabric-covered wind turbine blade. *Adv. Compos. Mater.* **2019**, *28*, 607–623. [CrossRef]
12. Fagan, E.M.; de la Torre, O.; Leen, S.B.; Goggins, J. Validation of the multi-objective structural optimization of a composite wind turbine blade. *Compos. Struct.* **2018**, *204*, 567–577. [CrossRef]
13. Yang, J.; Peng, C.; Xiao, J.; Zeng, J.; Xing, S.; Jin, J.; Deng, H. Structural investigation of composite wind turbine blade considering structural collapse in full-scale static tests. *Compos. Struct.* **2013**, *97*, 15–29. [CrossRef]
14. Kong, C.; Bang, J.; Sugiyama, Y. Structural investigation of composite wind turbine blade considering various load cases and fatigue life. *Energy* **2005**, *30*, 2101–2114. [CrossRef]
15. Paquette, J.; van Dam, J.; Hughes, S. Structural testing of 9 m carbon fiber wind turbine blade research blades. In Proceedings of the 45th AIAA Aerospace Sciences Meeting and Exhibit, Reno, NV, USA, 8–11 January 2007.
16. Jensen, F.M.; Falzon, B.G.; Ankersen, J.; Stang, H. Structural testing and numerical simulation of a 34 m composite wind turbine blade. *Compos. Struct.* **2006**, *76*, 52–61. [CrossRef]
17. Yang, B.; Sun, D. Testing, inspecting and monitoring technologies for wind turbine blades: A survey. *Renew. Sustain. Energy Rev.* **2013**, *22*, 515–526. [CrossRef]
18. Zhou, H.F.; Dou, H.Y.; Qin, L.Z.; Chen, Y.; Ni, Y.Q.; Ko, J.M. A review of full-scale structural testing of wind turbine blades. *Renew. Sustain. Energy Rev.* **2014**, *33*, 177–187. [CrossRef]
19. Yoo, C.; Son, E.; Hwang, S.; Kim, D.; Kim, S. 10 kW wind turbine blade aerodynamic design and verification. *J. Aerosp. Syst. Eng.* **2017**, *6*, 42–49.
20. International Electrotechnical Commission (IEC). *IEC 61400-1 Ed.3 Wind Turbines–Part 1: Design Requirements*; IEC: Geneva, Switzerland, 2005.
21. Jonkman, J.M.; Buhl, M.L., Jr. *FAST User's Guide*; NREL/EL-500-38230; National Renewable Energy Laboratory: Golden, CO, USA, 2005.

22. Churchfield, M.J.; Lee, S.; Michalakes, J.; Moriarty, P.J. A numerical study of the effects of atmospheric and wake turbulence on wind turbine dynamics. *J. Turbul.* **2012**, *12*, N14. [CrossRef]
23. Nandi, T.N.; Herring, A.; Brasseur, J.G. Non-steady wind turbine response to daytime atmospheric turbulence. *Phil. Trans. R. Soc. A* **2017**, *375*, 20160103. [CrossRef] [PubMed]
24. Yu, W. *VABS Manual for Users*; Utah State University: Logan, UT, USA, 2013.